Low-Profile Dual-Band Dual-Polarized Transmitarray Antenna Based on Multilayer Frequency Selective Surfaces

Raffaele De Marco, Emilio Arnieri, *Member, IEEE,* Francesco Greco, *Member, IEEE*, Arman Bordbar, Giandomenico Amendola, *Senior Member, IEEE*, and Luigi Boccia, *Senior Member, IEEE*

***Abstract*— In this work, a new dual-band dual-polarized transmitarray (TA) antenna element based on multilayer frequency selective surfaces is introduced. This novel configuration has been successfully tested for K/Ka satellite communication (SatCom) frequency bands and is composed of a single low-profile printed circuit board incorporating five metal layers without any vertical transitional elements. In contrast to existing solutions, this proposal eliminates the need for vertical interconnections, air gaps, or spacers between the metal layers, resulting in a cost-effective board with an overall thickness of 0.24 λ at 30 GHz. The proposed unit cell operates at 20 and 30 GHz exploiting an interleaved lattice configuration. It affords independent control of the transmitted field phase within a range of 300°, at both frequency bands while maintaining a transmission loss not exceeding 3.5 dB. To substantiate the proposed design, an 87 × 87 mm^2 TA has been prototyped and experimentally validated. The measured results indicate a peak gain of 20.6 and 22.8 dB at 20 and 30 GHz, respectively. Furthermore, the −1 dB gain bandwidth has been found to be 5% in the first band and 4.5% in the second band.**

***Index Terms*— Circularly polarized (CP) wave, dual-band antenna, Ka-band, satellite communications (SatComs), transmitarray (TA) antenna.**

I. Introduction

IN RECENT years, the Ka-band satellite communication (SatCom) sector has garnered significant attention due to its numerous advantages, including wider spectrum availability, higher data rates, compact terminal sizes, and simplified technology for multiple beam satellites [1]. The Ka-band frequency spectrum enables high bandwidth data transmission with throughputs up to 5 Gbps for consumer applications and even higher data rates for government or enterprise customers. The relevance of these frequency bands for SatCom applications will be further reinforced by the upcoming telecommunication infrastructure where K/Ka SatCom links will play a crucial role in facilitating the implementation of a nonterrestrial network [2], [3].

K/Ka-band satellites are based on bidirectional communications covering the range of 17.7–21.2 GHz for downlink (DL) and 27–31 GHz for uplink (UL), leading to an increase in research for the investigation of new solutions for dual-band antenna systems. In line with this trend, various antenna designs have been proposed in literature over the past few years, including several examples of dual-band Reflectarray (RA) and Transmitarray (TA) antennas. RA and TA gained popularity due to their advantages over traditional array antennas and reflectors. They can provide high gain without the need for complex feeding networks or bulky structures, and their manufacturing process is cost-effective. Compared to RA, where the feed is in front of the antenna aperture, TA antennas offer higher efficiency avoiding feeding blockage losses. Research studies on TA are rapidly evolving, especially in view of their possible application for K/Ka SatCom systems, where they can play a crucial role in ground terminals and in other nodes of the nonterrestrial network.

Similar to what happens in RA antennas, the most relevant challenge faced by dual-band TA is the creation of unit cells that can independently control their transmission phase in both frequency bands while maintaining the lowest possible insertion loss. Dual-band TA antennas are typically implemented using interleaved radiating elements, each of which is designed to manipulate wave propagation in one of the operating bands. In the context of K/Ka SatCom antenna systems, the radiators must also be dual-polarized to support circular or dual-linear polarization. There are two common approaches to designing dual-band TA antennas, namely, the multilayer frequency selective surface (M-FSS) approach and the receiver-transmitter architecture approach. In the M-FSS approach, multiple frequency selective surfaces [4] based on interleaved single-band radiating elements are separated by air gaps or thick substrates to achieve a wide transmission phase range, as shown in [5], [6], [7], [8], and [9]. For example, in [5], a dual-band circularly polarized M-FSS TA for SatCom applications is reported. This configuration makes use of three metal and dielectric layers separated by a 3.6 mm air gap. The major drawback of M-FSS-based TA is the increased thickness, manufacturing cost, and reliability due to a heterogeneous stack-up, which can be as thick as 0.55 to 1 wavelength (λ_o) at the center frequency of the highest band.

Manuscript received 1 March 2023; revised 10 May 2023; accepted 8 July 2023. Date of publication 21 July 2023; date of current version 6 September 2023. This work was supported by the European Commission Horizon 2020 Program through the Project FLEXCOM under Grant 101004233. *(Corresponding author: Raffaele De Marco.)*

Raffaele De Marco, Emilio Arnieri, Arman Bordbar, Giandomenico Amendola, and Luigi Boccia are with the Millimeter-wave Antennas and Integrated Circuits Laboratory (MAIC-Lab), Department of Computer Science, Modeling, Electronics and Systems Engineering (DIMES), University of Calabria, 87036 Rende, Italy (e-mail: raffaele.demarco@dimes.unical.it; emilio.arnieri@unical.it; arman.bordbar@dimes.unical.it; g.amendola@dimes.unical.it; luigi.boccia@unical.it).

Francesco Greco is with Antecnica, University of Calabria, 87036 Rende, Italy (e-mail: francesco.greco@antecnica.it).

Color versions of one or more figures in this article are available at https://doi.org/10.1109/TAP.2023.3296257.

Digital Object Identifier 10.1109/TAP.2023.3296257

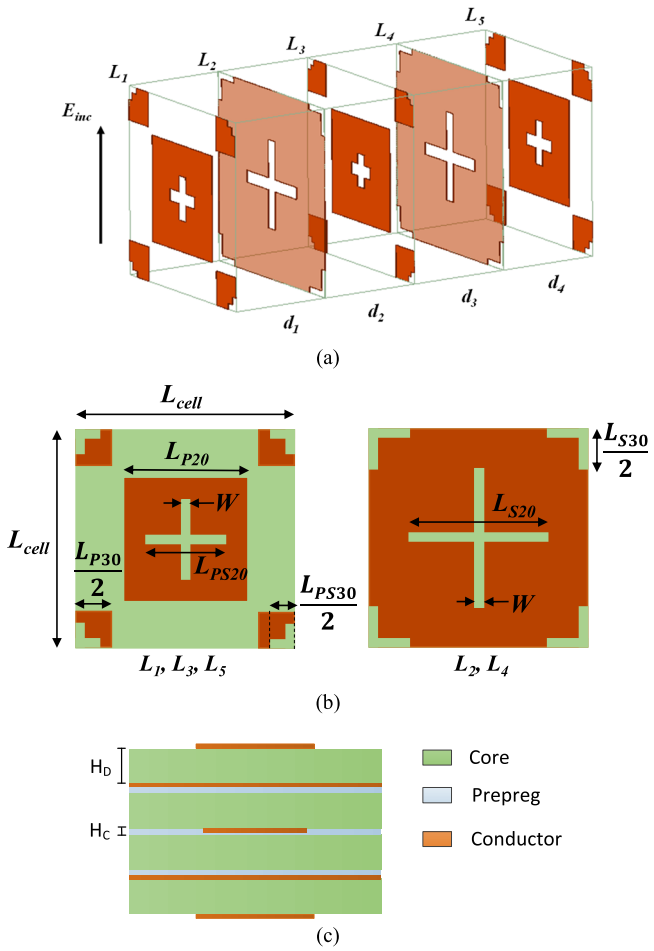

Fig. 1. (a) Dual-band TA unit-cell architecture, (b) geometrical parameters, and (c) stackup.

In contrast, the transmitter-receiver TA architecture approach offers a low-cost and compact solution, which eliminates the requirement for air gaps or thick substrates. Instead, it employs an array of receiving elements that are interconnected with another array of transmitting elements, all printed on a single printed circuit board. This results in a more compact design compared to the M-FSS approach, but on the other hand, it requires vertical interconnections, and it has not been proved yet for dual-band dual-polarized configurations. For example, in [10] a K/Ka single-bit TA is proposed using orthogonal polarizations in the two bands. This configuration operates as a dual-linearly polarized TA, and it requires five metal layers metallized via holes. In order to reduce the number of metal layers to 3, another example of the same configuration is reported in [11], where an interleaved arrangement is employed. Besides being both examples dual-linearly polarized, their efficiency is limited mainly because of the one-bit phase range resolution. Moreover, for many applications such as SatComs, they need to be combined with LP-to-CP polarization converters [12]. A similar approach was reported in [13], where a dual-band circularly polarized TA was introduced for Ku-band applications. Despite offering an improved efficiency of 32%, the effectiveness of this configuration has only been proved under conditions where the difference between the two operating bands is limited.

In this manuscript, a novel M-FSS cell topology is introduced for the dual-band dual-polarized operation at frequencies of 20 and 30 GHz. This cell topology is found to possess additional and unique advantages over the existing solutions in the field as it is the firstly reported dual-band dual-polarized M-FSS, which does not require air gaps or thick substrates. Yet it preserves the independency of control at the two frequency bands. As shown in Fig. 1, each TA cell is designed as a dual-band passband filter, and it is integrated onto a single printed circuit board with a total thickness of 0.24 λ_o in the upper-frequency band. The validation demonstrator was designed to cover the K/Ka-band SatCom frequencies. The proposed concept is based on an interleaved lattice employing stacked patch antennas coupled through crossed slots. Thanks to this solution, the phase of the transmitted field can be controlled within a 300° phase range.

The organization of the article is as follows. Section II provides an introduction to the TA unit cell, including the presentation of an equivalent circuit model. Section III utilizes the dual-polarized dual-band cell to design a TA test vehicle and reports on the experimental validation results. Finally, conclusions are discussed in Section IV.

II. Dual-Band Dual-Polarized Unit Cell Design

In the design of a single-band TA unit cell, two key parameters are the transmitted power and the phase range achievable by the unit cell. In the case of a dual-band unit cell, an additional requirement is necessary: independence between the two bands. It is indeed crucial to have independent phase control at each frequency band, meaning that any variation in the geometrical parameters that control the phase in one band should not impact the response of the unit cell at the other band. The approach employed in this work to attain this autonomy is to have a unit cell exhibiting a dual-band bandpass filter-like behavior with a high rejection level between the two bands. To this end, the utilization of an M-FSS TA cell, based on interleaved radiators, is deemed as a viable solution in this study.

M-FSS TA final performance depends on a variety of parameters, the most relevant ones being the number of layers, the type of substrate materials, and the layer separations. In [14], a comprehensive analytical assessment is presented, which substantiates the intrinsic limitation of this methodology. This analysis demonstrates that a minimum of three layers of resonators in the FSS is required to achieve a complete phase range of 360° with an insertion loss of 3 dB, thus providing a theoretical constraint. Typically, a 90° interlayer electrical separation is utilized to attain the full phase range in M-FSS; however, this approach results in a thick and complex structure where air gaps are utilized as the interlayer spacing to mitigate losses. The implementation of an inhomogeneous stack-up not only results in a bulky structure but also renders the system vulnerable to mechanical instability and prone to possible thermal deformations.

The current study derives from the single-band FSS configuration described in [15], which is comprised of two identical patch antennas connected via a central slot. This configuration exhibits a dual resonant response, with one resonance

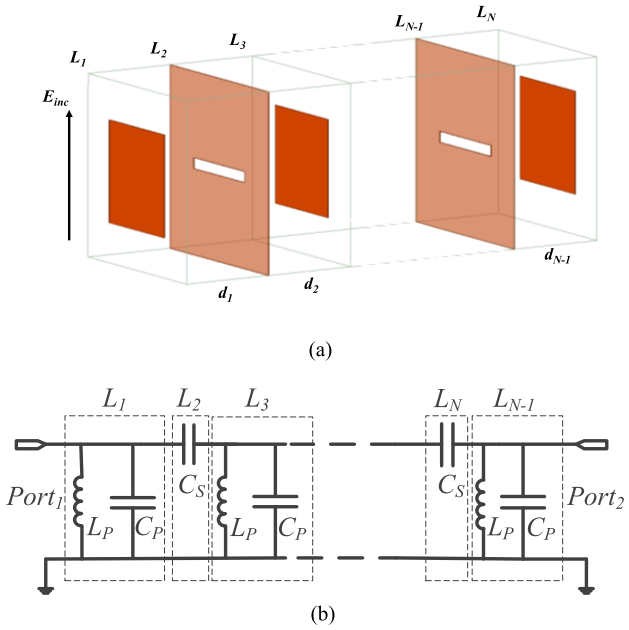

Fig. 2. (a) N-layer single-band single-pol TA unit-cell configuration and (b) its equivalent circuit model.

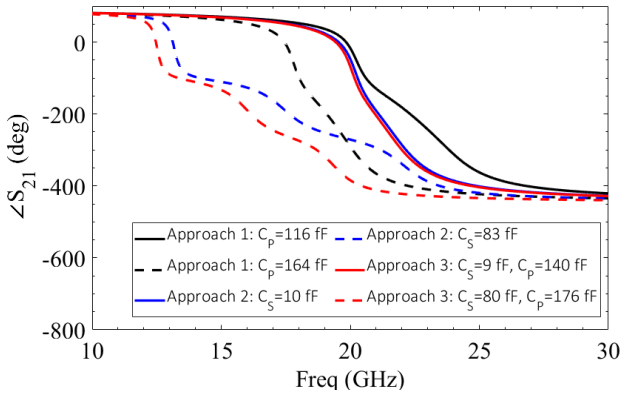

Fig. 3. Transmission coefficient phase response of the five-layer circuit for different phase control approaches. Approach 1: varying the resonator resonant frequency by manipulating C_P while having $L_P = 0.38$ nH and $C_S = 22$ fF. Approach 2: varying the coupling capacitor, C_S, while having $C_P = 136$ fF and $L_P = 0.38$ nH. Approach 3: varying both the coupling and the resonators' capacitor (i.e., C_P and C_S) while having $L_P = 0.38$ nH.

originating from the resonators and the other resulting from the interaction between the resonators and the coupling slot. While the use of three metal layers (consisting of two layers embedding resonators and one layer for coupling) is sufficient to achieve acceptable behavior as an FSS, it does not enable complete control over the phase of the transmitted field; therefore, in this study, a generalized design methodology is proposed to expand upon this approach by incorporating N metal layers. As will be shown, the proposed approach confers several benefits, including increased flexibility in the interlayer separation distance, which is no longer restricted to a quarter wavelength; furthermore, the high level of selectivity synergizes with the ability to effectively arrange the radiators in an interleaved configuration. As will be shown, these properties will be essential for the design of a dual-band dual-polarized TA.

The proposed design methodology is first introduced by analyzing a single-band, single-polarization TA cell using its equivalent circuit model. In a second incremental step, the dual-band dual-polarized structure is analyzed.

A. Single-Band Single-Pol M-FSS TA Unit-Cell

The generalized model of the single-band single-polarization M-FSS TA cell is reported in Fig. 2(a). The configuration is structured as a cascade of N-metal layers interleaved by N-1 dielectrics that have identical characteristics and thicknesses. Specifically, the dielectric thickness is equal to d, while the relative permittivity and loss tangent are equal to 3.66 and 0.004, respectively. The metal layers with an odd index in the proposed design ($L_1 L_3, \ldots$) contain a patch antenna. The layers with even index ($L_2, L_4, \ldots$) serve as ground planes where a rectangular slot is etched to provide coupling between two adjacent patches. The multilayer structure acts as a passband filter where each patch is a resonator. By extending the approach proposed in [15], the M-FSS unit cell can be analyzed using the simplified equivalent circuit reported in Fig. 2(b), where dielectric and conductor losses are not taken into account. Each patch can be modeled as an L-C tank, whereas the slots are represented through a coupling capacitor C_S. This circuit thus behaves as a capacitively coupled bandpass filter [16]. In a first assumption, the values of the lumped components remain identical for all layers. The application of an equivalent circuit was initially undertaken to determine the relationship between the number of layers and the transmission phase range. The lumped circuit values were estimated following the approach given in [16] under the assumption of a Chebyshev response with a 2 dB ripple and a 6 GHz bandwidth. As expounded in [17], the phase range is associated with the final system bandwidth. Hence, the application at hand warrants a configuration with $N = 5$ to meet the desired requirements; the phase range estimated is about 330°.

Upon determination of the desired number of layers, an analysis of the proposed circuit is conducted to assess its viability for TA applications. Specifically, the focus is on ascertaining how the transmitted field phase can be manipulated. Various techniques can be employed to control the phase. The predominant approach (referred to as *Approach 1*), as documented in the literature, involves varying the resonator response through the variation of its resonant frequency (i.e., L_P or C_P). Some examples of design that adopt this approach with the respective equivalent circuit are shown in [18], [19], and [20]. As reported in Fig. 3, a change of C_P while having L_P and C_S fixed provides a phase range of about 270° while the passband remains approximately the same. An alternative method (*Approach 2*) is to maintain the resonator fixed and to change the coupling capacitor only, C_S. In this case, the achieved phase range is 220°, and the passband profile is altered. The effect of a combination of both techniques (*Approach 3*) leads to a phase range of 330° within an insertion loss of 3 dB. Although the implementation of the circuit

Fig. 2(b) can be accomplished directly using the geometry reported in Fig. 2(a), an alternative approach based on square patches loaded with a rectangular slot was favored, given the aim of expanding the model into a dual-band dual-polarized cell. As will be shown, this approach allows tuning the patch resonant frequency while keeping fixed its length, L, and enabling an effective implementation of the dual-band dual-polarized TA cell by using an interleaved arrangement. The circuit of Fig. 2(b) can be converted into the geometry of Fig. 2(a) using different procedures. Once the dielectric characteristics are defined, the first step is defining the geometrical parameters of the slot-loaded square patch [21]. Among the different combinations of patch and slot length, the ideal arrangement should be determined based on the capability to attain the maximum phase range by manipulating solely the slots' length, namely L_{PS} and L_S. Besides, there are various approaches available for determining the geometry of the coupling slot. The interactions of the different elements of the M-FSS TA cell create mutual dependences, which can be simplified by fixing some geometrical relations. To keep the control of the transmitted phase as simple as possible, the slots etched on the patch surface and the coupling slots are related as follows: the length of the slots loading the patches is set to be half of the length of the coupling slots, that is, $L_{PS} = L_S/2$. As a result, each single-band linearly polarized M-FSS TA cell is regulated by a single parameter, governing its transmitted phase through alterations in both resonator frequency and coupling intensity.

To emulate this behavior in the M-FSS TA cell, the length of the patches and loading slots located in the inner layers should undergo a slight tuning to make them resonate at the same frequency, despite the differences in the effective dielectric permittivity across the different layers.

Following the outlined design approach, an M-FSS TA cell was designed with $N = 5$ having a center band frequency of 20 GHz. The PCB stackup comprises five metals layers and four identical dielectric substrates of 0.508 mm Rogers RO4350 with a relative permittivity of 3.66 and dielectric loss tangent of 0.004. Fig. 4 presents a comparison between the equivalent circuit and full-wave simulated transmission coefficient. The latter approach was implemented in an infinite array setting. Simulated results are reported for three distinct configurations, representing the nominal configuration, as well as the two extremes of the L_S range. Results reveal a good agreement between the two simulation techniques. Nonetheless, a key distinction between them pertains to the full-wave simulation's identification of resonance at about 25 GHz. This behavior, resulting from the periodicity effect [22], is not captured by the equivalent circuit approach, and it increases the phase range.

The simulation results indicate a phase range of 300° with transmission losses not exceeding 3 dB. Hence, the full-wave simulated phase range is in line with the ones predicted by the circuital model.

B. Dual-Band Dual-Polarized M-FSS TA Unit-Cell

To generate dual–polarization, cross-shaped slots are employed in place of the rectangular slots both to load the patch and for coupling. As reported in [23], this technique gives an isolation of about 30 dB between the vertical and horizontal polarization. Such a level of isolation is adequate to control the two polarizations independently. In the present work, the transmitted field phase is equal for both polarizations, resulting in symmetrical slots.

Thanks to the good selectivity of the M-FSS TA cell presented in Section II-A, concurrent operation across two distinct frequency bands can be obtained by interleaving the lower frequency cell with the higher frequency one. For the application at hand, the 20 GHz (DL) TA cell can be interleaved with four 30 GHz (UL) ones having the same configuration. Given the high frequency separation between the two bands, it is not difficult to optimize the patch geometry to have an isolation of higher than 35 dB between the two

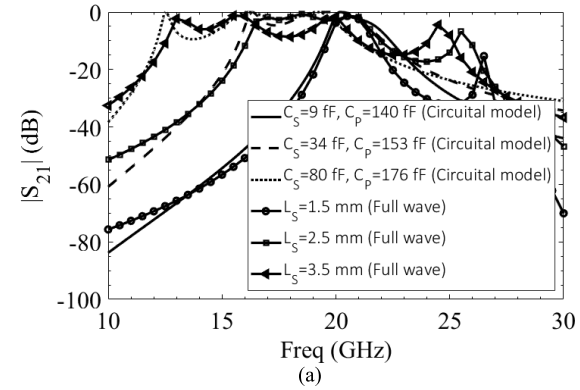

(a)

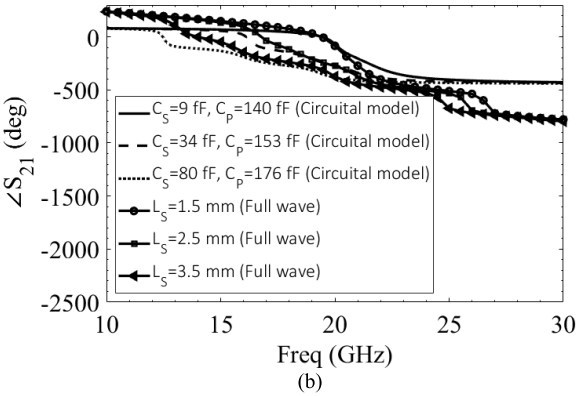

(b)

Fig. 4. Comparison between the circuital model transmission coefficient response and simulated for three different slot lengths (a) magnitude and (b) phase.

TABLE I
KEY GEOMETRICAL PARAMETERS OF THE DUAL-BAND DUAL-POL TA UNIT CELL SHOWN IN FIG. 1

Parameters	Value (mm)	Variables	Range (mm)
L_{CELL}	5.8	L_{S20}	1.5-4
W	0.35	L_{S30}	1-2.1
H_D	0.508	L_{PS20}	0.75-2
H_P	0.1	L_{PS30}	0.5-1.05
L_{P20}	3.25*		
L_{P30}	2.1*		

*For the patches of the inner layer (L3) L_{P20}=3.15 mm and L_{P30}=1.9 mm.

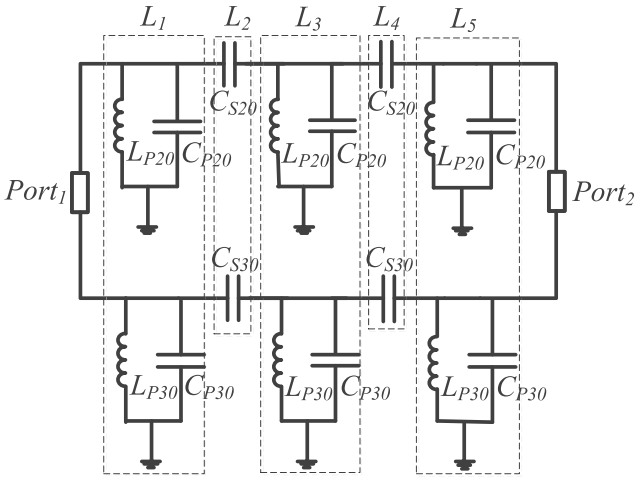

Fig. 5. Dual-band unit-cell equivalent circuit model.

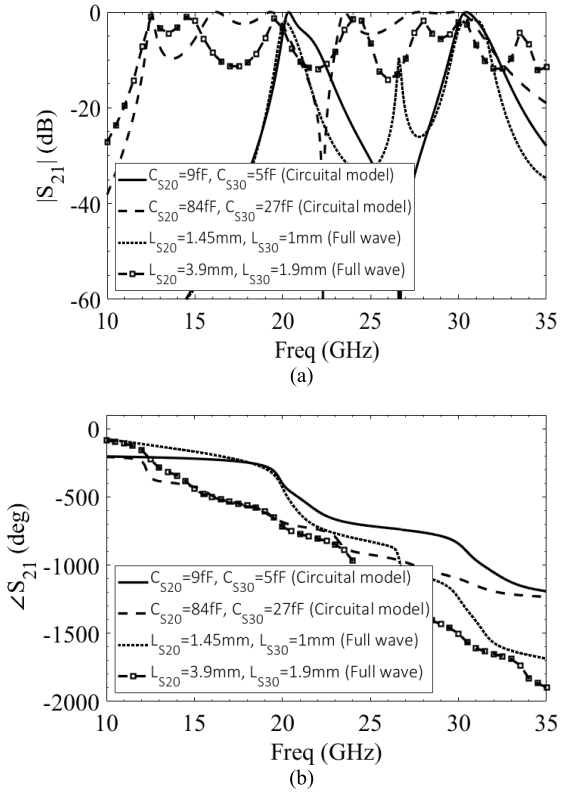

Fig. 6. Circuital model and full-wave transmission coefficient response: (a) amplitude and (b) phase. (C_{R20} = 135 fF, L_{R20} = 0.38 nH, C_{R30} = 104 fF, L_{R30} = 0.23 nH).

bands. An advantage of the present design is that modifications to the outer perimeter of the patch are not required to manipulate the transmitted phase. As a result, cross-frequency coupling remains relatively stable during phase adjustment, thereby facilitating the independent design of the TA cell for each frequency band. Fig. 1 illustrates the dual-band dual-polarized configuration, while Table I presents all pertinent dimensions. The corresponding equivalent circuit is depicted in Fig. 5 alongside the transmission coefficient response simulated using the circuital model and the full-wave analysis.

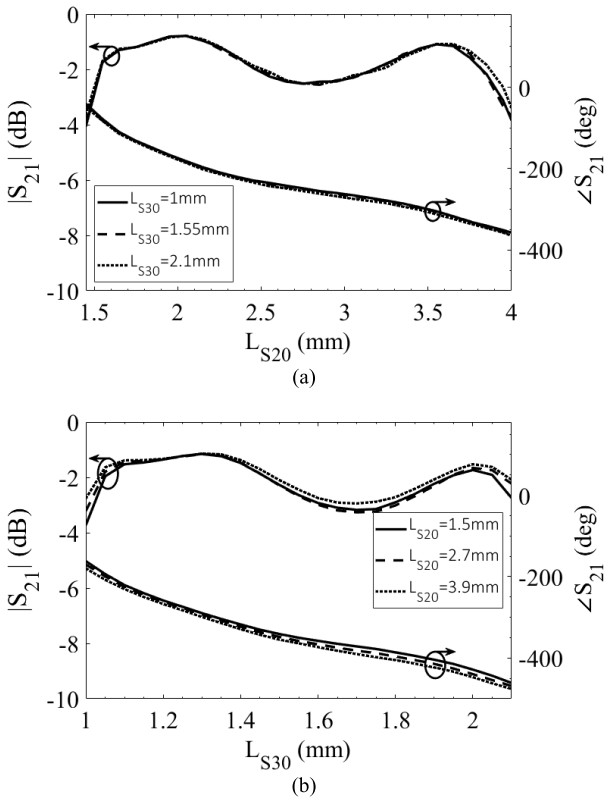

Fig. 7. Simulated transmission response of the dual-band dual-polarized TA unit cell with respect to the phase control parameters at: (a) 20 GHz and (b) 30 GHz.

Fig. 6 the phase range within a 3 and 3.5 dB insertion loss is about 300° at both 20 and 30 GHz. The amplitude and phase characteristics of the TA unit cell as functions of the phase control parameters at 20 and 30 GHz are presented in Fig. 7.

The maximum phase error is 6° and 20° at 20 and 30 GHz, respectively. The amplitude variations remain below 0.7 dB at both bands. Thereby, the two frequencies operate independently, as changes to L_{PS30} minimally impact the phase response at 20 GHz, while modifications to L_{PS20} similarly exert negligible influence on the cell response at 30 GHz. In TA design, it is also essential to account for the sensitivity of unit cell amplitude and phase to changes in the angle of incidence. Fig. 8 depicts the transmission coefficient response for a range of angles of incidence. The transmission response of the unit cell exhibits a degree of robustness up to an angle of incidence of 30°. Alterations to the angle of incidence do not significantly affect the phase response at either 20 or 30 GHz. Tt 20 GHz, an attenuation in magnitude response, however, occurs with increasing angle of incidence for L_{S20} values approximately 2.7 mm. At 30 GHz, a more pronounced sensitivity to the angle of incidence is observed at the extremes of L_{S30} range, resulting in a maximum reduction of approximately 2 dB. This heightened sensitivity, coupled with substrate and prepreg losses, accounts for the disparity in TA efficiency between the 20 and 30 GHz frequency bands.

III. Fabrication, Measurements, and Results

To validate the dual-band dual-polarized M-FSS TA cell proposed in the previous section, a 421-element prototype was

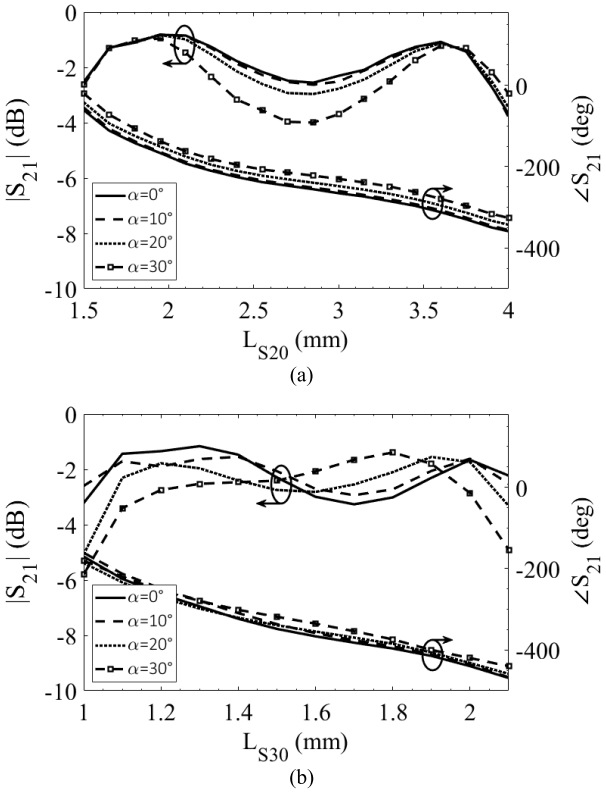

Fig. 8. Unit-cell transmission coefficient response for different angles of incidence at (a) 20 and (b) 30 GHz.

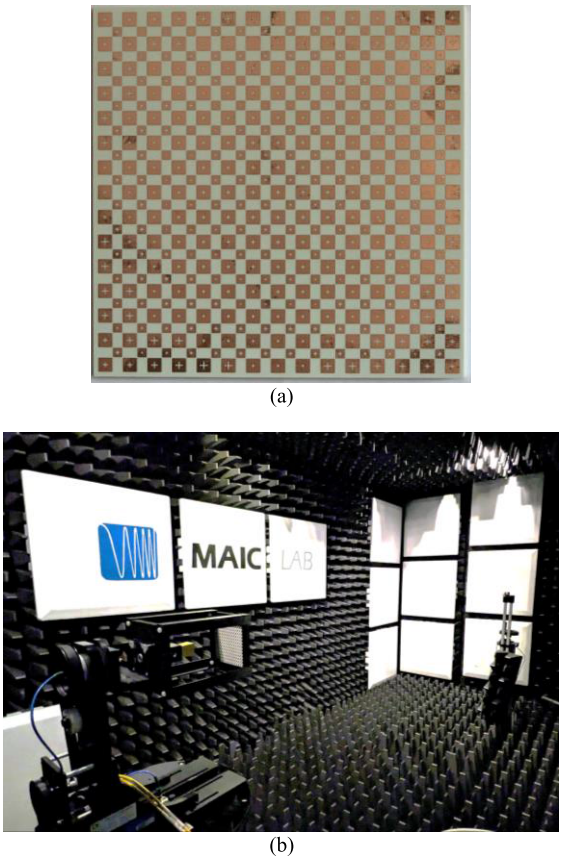

Fig. 9. Dual-band dual-polarized M-FSS TA prototype: (a) top view and (b) mounted in the receiving mast of the anechoic chamber available at the MAIC-LAB, at the University of Calabria, Italy.

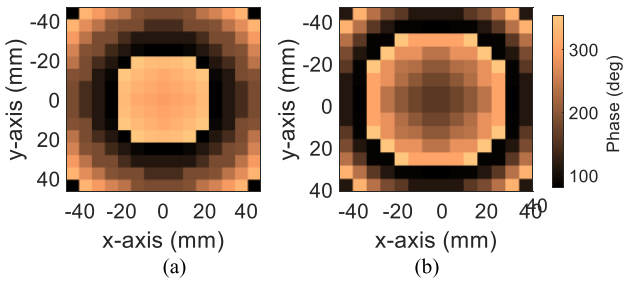

Fig. 10. Phase distribution on the TA elements: (a) DL (20 GHz) and (b) UL (30 GHz).

designed and experimentally characterized. The TA consists of two subarrays: a UL array comprising 196 elements arranged in a 14 × 14 square lattice and a DL array containing 225 elements organized in a 15 × 15 square matrix. Fig. 9(a) The total physical dimensions of each prototype measure 87 × 87 mm, with a 10-mm extension along the edges to provide mechanical support. The prototype stack-up is reported in Fig. 1(c). Each dielectric layer includes a Rogers RO4350 slab having a thickness of 0.508 mm and an I-TERA MT 3313 prepreg layer, the thickness of which is equal to 0.1 mm.

A dual-polarized quad-ridged horn antenna, RFecho ODPA-180400-20 mm, covering both K and Ka bands, is used to illuminate the TA. The E-plane HPBW of the feed at 20 GHz is 38.5° while on H-plane is 50°; at 30 GHz, the HPBW is 27° and 37° on the E-plane and H-plane, respectively. The focal distance was optimized to attain an optimal balance between spill-over loss and illumination efficiency for both frequency bands. The TA design and optimization were performed using an in-house simulation tool developed following the approach described in [24]. An optimal focal distance of 80 mm was determined to yield the most favorable results, corresponding to a F/D ratio of 0.65. Such a selection resulted in an illumination level below −10 and −13 dB at the edges and corners of the TA, respectively. To calculate the focal distance properly the analytical method shown in [25] has been used. In this case, the pattern of each element has been modeled by a $\cos(\theta)$ while the pattern of the feed has been modeled by $cos^{qE}(\theta)$ and $cos^{qH}(\theta)$ for E-plane and H-plane, respectively. At 20 GHz, $qE = 6$ and $qH = 3$, instead at 30 GHz, $qE = 10$ and $qH = 6$. Besides, a full-wave analysis [26] of the TA was also performed, including the actual geometry of the dual-polarized feed. The TA prototype was designed to have both beams pointing in the broadside direction. The phase distribution of each TA cell for the UL and DL frequencies is reported in Fig. 10.

A. Experimental Results

The TA radiation performance in both UL and DL bands was measured in the anechoic chamber of the MAIC LAB at the University of Calabria Fig. 9(b). Figs. 11 and 12 show the co- and cross-polar far-field E-plane and H-plane radiation patterns at 20 and 30 GHz, respectively. Measured results are compared with full-wave and analytical simulations showing a

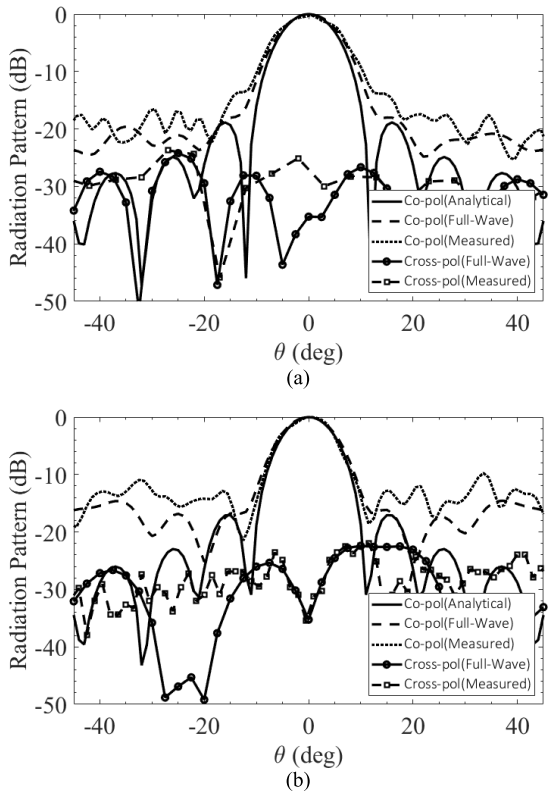

Fig. 11. Simulated and measured co- and cross-polar far-field. (a) E-plane and (b) H-plane radiation pattern at 20 GHz.

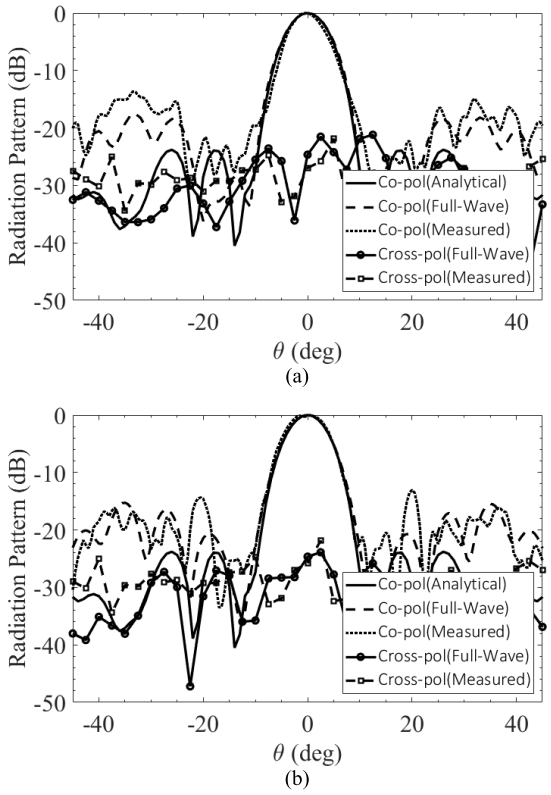

Fig. 12. Simulated and measured co- and cross-polar far-field. (a) E-plane and (b) H-plane radiation pattern at 30 GHz.

TABLE II
COMPARISON BETWEEN THE PROPOSED DESIGN AND OTHER WORKS

Ref.	Center Freq. (GHz)	Overall Thickness	Pol.	Aperture Efficiency (%)	Gain BW (%)	
					-1 dB	-3 dB
[5]	20/30	0.68λ_o	CP	10/6	-	10/7
[6]	12.5/14.25	0.55λ_o	Dual Pol	38/46	-	4.2/6.3
[7]	13.5/22	0.66λ_o	Dual Pol	34/27	6/6	-
[8]	11/12.5	0.5λ_o	Dual Pol	38/34	6.8/5.4	-
[10]	19.8/29.1	0.25λ_o	Dual LP	25.1/20	-	19.8/12
[11]	20/30	0.17λ_o	Dual LP	21.2/20.1	10.7/8.3	11.3/11.4
[13]	12/14.2	0.075 λ_o	CP	32.2/28.9	-	7.5/7
This work	20/30	0.24 λ_o	Dual Pol	27/23	5/4.5	8.8/8.3

good agreement. The results reveal that the measured sidelobe levels at 20 GHz are approximately −14 dB on the E-plane and −10 dB on the H-plane, while at 30 GHz, their levels are roughly equivalent to −14 and −13.5 dB on the E-plane and H-plane, respectively.

The measured cross-polar field remains below −25 dB in both the DL and UL bands. It has also been verified that lower sidelobe levels, similar to the ones predicted by the analytical model, could be achieved by using two single-band feeds.

The simulated and measured gain versus frequency is shown in Fig. 13. The measured peak gain in the DL band is 20.64 dB corresponding to an aperture efficiency of 27%. The −1 dB

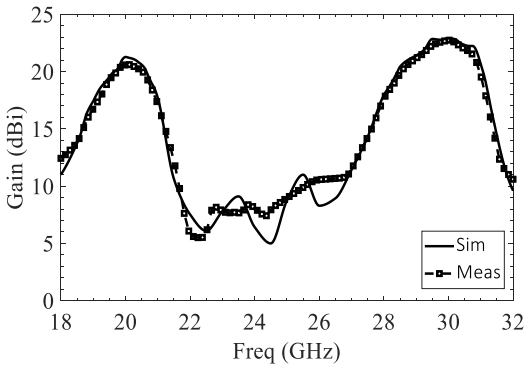

Fig. 13. Simulated and measured gain versus frequency.

gain bandwidth is 1 GHz (5% at the center frequency). A peak gain of 22.8 dB has been obtained in the UL band, showing an aperture efficiency of 23%. A −1 dB gain bandwidth of 4.5% is achieved, corresponding to 1.35 GHz. It is worth noticing that the maximum discrepancy between the measured and simulated gain is approximately 0.7 dB in both bands.

The performance of the proposed design is compared with other TA configurations in Table II. Limiting the comparison with other dual-band dual-polarized TAs, namely [5], [6], [7], and [8], the proposed configuration has a significantly thinner profile by at least 50%. The efficiency is also improved when compared to [5], which operates in the same band. Other TA designs reported in Table II, namely [10] and [11], exhibit a comparable profile but are dual-linearly polarized and have lower aperture efficiency due to their 1-bit phase resolution. In contrast, the example in [13] can be only utilized for circular

polarization and covers a different frequency range. Thus, among the aforementioned works, the proposed antenna offers the best compromise between overall thickness and aperture efficiency for dual-band dual-polarized TAs at Ka band.

IV. Conclusion

The present study introduced a novel dual-band dual-polarized TA architecture that employs multilayer frequency selective surfaces. The proposed design approach enables a low-cost and low-profile implementation utilizing a single multilayer PCB without any air gap or vertical transition.

An equivalent circuit model for the unit cell has been formulated and examined, providing insight into the optimal phase control methodology and the transmission mechanism. It was found that a phase tuning range of 300° for both polarizations and operating bands can be achieved using a PCB with five metal layers.

A TA prototype has been manufactured and measured to validate the proposed TA unit cell. An aperture efficiency of 27 and 23% has been measured at 20 and 30 GHz, respectively, whereas a -1 dB gain bandwidth of about 5 % is reported for the DL band and 4.5% for the UL band.

The proposed methodology is based on the incorporation of DL and UL unit cells that are interleaved and possess autonomous control over the transmitted phase for each band and polarization. This approach yields a considerable reduction in the complexity of the design process. Furthermore, the proposed unit cell and TA are versatile in their ability to scale with varying frequencies and are well suited to implement other dual-band TAs that operate in two distinct frequency bands characterized by a substantial difference in upper and lower frequencies.

References

[1] D. Venugopal, C. Muthugadahalli, and K. Narayanan, "Ka band satellite communication systems—Applications and configurations," in *Proc. Int. Astron. Congr. (IAC)*, 2015, pp. 12–16.

[2] A. Sattarzadeh et al., "Satellite-based non-terrestrial networks in 5G: Insights and challenges," *IEEE Access*, vol. 10, pp. 11274–11283, 2022, doi: 10.1109/ACCESS.2021.3137560.

[3] F. Lu et al., "System demonstrations of Ka-band 5-Gbps data transmission for satellite applications," *Int. J. Satell. Commun. Netw.*, vol. 40, no. 3, pp. 204–217, May 2022, doi: 10.1002/sat.1434.

[4] A. H. Abdelrahman, F. Yang, A. Z. Elsherbeni, and P. Nayeri, "Analysis and design of transmitarray antennas," *Synth. Lectures Antennas*, vol. 6, no. 1, pp. 1–175, Jan. 2017, doi: 10.2200/s00749ed1v01y201612ant012.

[5] H. Hasani, J. S. Silva, S. Capdevila, M. García-Vigueras, and J. R. Mosig, "Dual-band circularly polarized transmitarray antenna for satellite communications at (20, 30) GHz," *IEEE Trans. Antennas Propag.*, vol. 67, no. 8, pp. 5325–5333, Aug. 2019, doi: 10.1109/TAP.2019.2912495.

[6] A. Aziz, F. Yang, S. Xu, M. Li, and H.-T. Chen, "A high-gain dual-band and dual-polarized transmitarray using novel loop elements," *IEEE Antennas Wireless Propag. Lett.*, vol. 18, no. 6, pp. 1213–1217, Jun. 2019, doi: 10.1109/LAWP.2019.2912645.

[7] S. Yang, Z. Yan, X. Li, and M. Cai, "Dual-band dual-polarized transmitarray with independent control of polarization at each band," *Int. J. RF Microw. Comput.-Aided Eng.*, vol. 32, no. 2, pp. 1–10, Feb. 2022, doi: 10.1002/mmce.22957.

[8] M. O. Bagheri, H. R. Hassani, and B. Rahmati, "Dual-band, dual-polarised metallic slot transmitarray antenna," *IET Microw., Antennas Propag.*, vol. 11, no. 3, pp. 402–409, Feb. 2017, doi: 10.1049/iet-map.2016.0159.

[9] S. A. Matos et al., "High gain dual-band beam-steering transmit array for Satcom terminals at Ka-band," *IEEE Trans. Antennas Propag.*, vol. 65, no. 7, pp. 3528–3539, Jul. 2017, doi: 10.1109/TAP.2017.2702658.

[10] R. Madi, A. Clemente, and R. Sauleau, "Dual-band dual-linearly polarized transmitarray at Ka-band," in *Proc. 50th Eur. Microw. Conf. (EuMC)*, Jan. 2021, pp. 340–343, doi: 10.23919/EuMC48046.2021.9337962.

[11] K. T. Pham, R. Sauleau, E. Fourn, F. Diaby, A. Clemente, and L. Dussopt, "Dual-band transmitarrays with dual-linear polarization at Ka-band," *IEEE Trans. Antennas Propag.*, vol. 65, no. 12, pp. 7009–7018, Dec. 2017, doi: 10.1109/TAP.2017.2762011.

[12] P. Naseri, S. A. Matos, J. R. Costa, C. A. Fernandes, and N. J. G. Fonseca, "Dual-band dual-linear-to-circular polarization converter in transmission mode application to K/Ka-band satellite communications," *IEEE Trans. Antennas Propag.*, vol. 66, no. 12, pp. 7128–7137, Dec. 2018, doi: 10.1109/TAP.2018.2874680.

[13] Y.-M. Cai et al., "Dual-band circularly polarized transmitarray with single linearly polarized feed," *IEEE Trans. Antennas Propag.*, vol. 68, no. 6, pp. 5015–5020, Jun. 2020, doi: 10.1109/TAP.2019.2963594.

[14] A. H. Abdelrahman, A. Z. Elsherbeni, and F. Yang, "Transmission phase limit of multilayer frequency-selective surfaces for transmitarray designs," *IEEE Trans. Antennas Propag.*, vol. 62, no. 2, pp. 690–697, Feb. 2014, doi: 10.1109/TAP.2013.2289313.

[15] R. Pous and D. M. Pozar, "A frequency-selective surface using aperture-coupled microstrip patches," *IEEE Trans. Antennas Propag.*, vol. 39, no. 12, pp. 1763–1769, Dec. 1991, doi: 10.1109/8.121598.

[16] S. Cohn, "Direct-coupled-resonator filters," *Proc. IRE*, vol. 45, no. 2, pp. 187–196, 1957, doi: 10.1109/JRPROC.1957.278389.

[17] L. Boccia, I. Russo, G. Amendola, and G. Di Massa, "Multilayer antenna-filter antenna for beam-steering transmit-array applications," *IEEE Trans. Microw. Theory Techn.*, vol. 60, no. 7, pp. 2287–2300, Jul. 2012, doi: 10.1109/TMTT.2012.2195673.

[18] B. Rahmati and H. R. Hassani, "Low-profile slot transmitarray antenna," *IEEE Trans. Antennas Propag.*, vol. 63, no. 1, pp. 174–181, Jan. 2015, doi: 10.1109/TAP.2014.2368576.

[19] M. Niroo Jazi, M. R. Chaharmir, J. Shaker, and A. R. Sebak, "Broadband transmitarray antenna design using polarization-insensitive frequency selective surfaces," *IEEE Trans. Antennas Propag.*, vol. 64, no. 1, pp. 99–108, Jan. 2016, doi: 10.1109/TAP.2015.2500230.

[20] Q. Luo, S. Gao, M. Sobhy, and X. Yang, "Wideband transmitarray with reduced profile," *IEEE Antennas Wireless Propag. Lett.*, vol. 17, no. 3, pp. 450–453, Mar. 2018, doi: 10.1109/LAWP.2018.2794605.

[21] B. R. Vishvakarma, "Analysis of slot loaded microstrip patch antenna," in *Proc. IEEE Antennas Propag. Soc. Symp.*, Monterey, CA, USA, Mar. 2004, pp. 2420–2423, doi: 10.1109/APS.2004.1331861.

[22] R. Luebbers and B. Munk, "Some effects of dielectric loading on periodic slot arrays," *IEEE Trans. Antennas Propag.*, vol. AP-26, no. 4, pp. 536–542, Jul. 1978, doi: 10.1109/TAP.1978.1141887.

[23] C. H. Tsao, Y. M. Hwang, F. Kilburg, and F. Dietrich, "Aperture-coupled patch antennas with wide-bandwidth and dual-polarization capabilities," in *Proc. Int. Symp., Antennas Propag.*, Jun. 1988, pp. 936–939, doi: 10.1109/APS.1988.94241.

[24] A. Clemente, L. Dussopt, R. Sauleau, P. Potier, and P. Pouliguen, "Focal distance reduction of transmit-array antennas using multiple feeds," *IEEE Antennas Wireless Propag. Lett.*, vol. 11, pp. 1311–1314, 2012, doi: 10.1109/LAWP.2012.2227105.

[25] M. ŻŻebrowski. *Illumination and Spillover Efficiency Calculations for Rectangular Reflectarray Antennas*. Accessed: Nov. 28, 2022. [Online]. Available: http://highfrequencyelectronics.com/Dec12/1212_HFE_reflectarray.pdf

[26] *HFSS*, Ansys, Canonsburg, PA, USA, 2019.

Raffaele De Marco was born in Cosenza, Italy, in 1994. He received the B.E. and M.E. degrees in information technology and telecommunication engineering from the University of Calabria, Rende, Italy, in 2016 and 2019, respectively. He is currently pursuing the Ph.D. degree in information and communication technologies with the University of Calabria.

His current research interests include the design of reflectarrays, transmitarrays, and pattern reconfigurable antennas.

Emilio Arnieri (Member, IEEE) was born in Cosenza, Italy, in 1977. He received the M.E. degree (Hons.) in information technology engineering from the University of Calabria, Rende, Italy, in 2003, and the Ph.D. degree in electronics engineering from the University Mediterranea of Reggio Calabria, Reggio Calabria, Italy, in 2007.

He is currently an Assistant Professor with the Department of Informatics, Modeling, Electronics and System Engineering (DIMES), University of Calabria, where he has participated in several national, European Union, and ESA Projects. He has coauthored more than 90 articles published in international journals and proceedings of international conferences. His research interests include circular polarizers, the development of dual-band antennas and millimeter-wave components, synthetic aperture radar, and beam scanning antennas.

Dr. Arnieri was selected as a finalist for the Best Paper Award in Antenna Design at the 13th European Conference on Antennas and Propagation (EuCap 2019). He was a recipient of the Outstanding Associate Editor Awards assigned by the Editorial Board of the IEEE ANTENNAS AND WIRELESS PROPAGATION LETTERS in 2021. He is an Associate Editor for IEEE ANTENNAS AND WIRELESS PROPAGATION LETTERS, an Advisory Editor for the *Engineering Report*s (Wiley), and a Guest Editor for *Sensors* (MDPI) and *Electonics* (MDPI). He is the Co-Founder of the academic spin-off Antecnica.

Francesco Greco (Member, IEEE) was born in Cosenza, Italy, in 1988. He received the M.E. degree in telecommunication engineering and the Ph.D. degree in information and communications technology from the University of Calabria, Rende, Italy, in 2013.

He is currently a Research Fellow with the Department of Informatics, Modeling, Electronics and System Engineering, University of Calabria. He has coauthored different scientific publications in international journals and proceedings at international conferences. His research interests include satellite communications, dual-band antennas, and millimeter-wave components.

Dr. Greco is a member of the Societ Italiana di Elettromagnetismo (SIEm) and is the CEO of the academic spin-off Antecnica.

Arman Bordbar was born in BandarLengeh, Iran, in 1990. He received the M.E. degree in telecommunication engineering from the University of Shiraz, Shiraz, Iran, in 2016. He is currently pursuing the Ph.D. degree with the Department of Informatics, Modeling, Electronics, and System Engineering, University of Calabria, Rende, Italy.

He has coauthored several articles in international journals and proceedings of international conferences. His research interests include beamformer networks, ultrawideband antenna, terahertz metamaterial absorbers, and microwave component design.

Giandomenico Amendol (Senior Member, IEEE) received the M.E. degree in electrical engineering from the University of Calabria, Rende, Italy, in 1987.

From 1988 to 1992, he was a Research Fellow with the Proton Synchrotron Division, European Center for Nuclear Research, Geneva, Switzerland. He is currently an Associate Professor with the Department of Informatics, Modeling, Electronics and System Engineering, University of Calabria, where he is also the Director of the Millimeter-wave Antennas and Integrated Circuits (MAIC) Laboratory. His current research interests include antennas, phased arrays, and microwave and millimeter-wave circuits. He was responsible for numerous research projects funded by the European Union and the European Space Agency.

Prof. Amendola was an Associate Editor of IEEE TRANSACTIONS ON ANTENNAS AND PROPAGATIOn.

Luigi Boccia (Senior Member, IEEE) was born in Lungro, Italy, in 1975. He received the Ph.D. degree in electronic engineering from the University of Calabria, Rende, Italy, in 2000, and the Ph.D. degree in electronics engineering from the University Mediterranea of Reggio Calabria, Reggio Calabria, Italy, in 2003.

From 2005 to 2021, he was an Assistant Professor in electromagnetics with the University of Calabria, where he is currently an Associate Professor. He is the Co-Editor of the *Space Antenna Handbook* (Wiley, 2012). His current research interests include active antennas, reflectarrays, beam-scanning antennas, and microwave and mm-wave IC design.

Dr. Boccia is a member of the European Microwave Association (EuMA) and the Societá Italiana di Elettromagnetismo (SIEm). He serves as an Associate Editor for the IEEE MICROWAVE AND WIRELESS COMPONENTS LETTERS, the IEEE ANTENNAS AND WIRELESS PROPAGATION LETTERS and the *International Journal of Microwave and Wireless Technologies* (Cambridge University Press).

Open Access funding provided by 'Università della Calabria' within the CRUI CARE Agreement